NASA Technical Memorandum 100272

Vibration and Flutter Characteristics of the SR7L Large-Scale Propfan

Richard August
Sverdrup Technology, Inc.
Lewis Research Center
Cleveland, Ohio

and

Krishna Rao V. Kaza
Lewis Research Center
Cleveland, Ohio

January 1988

NASA

VIBRATION AND FLUTTER CHARACTERISTICS OF THE SR7L LARGE-SCALE PROPFAN

Richard August
Sverdrup Technology, Inc.
Lewis Research Center
Cleveland, Ohio 44135

and

Krishna Rao V. Kaza
National Aeronautics and Space Administration
Lewis Research Center
Cleveland, Ohio 44135

SUMMARY

An investigation of the vibration characteristics and aeroelastic stability of the SR7L Large-Scale Advanced Propfan has been performed using a finite element blade model and an improved aeroelasticity code. Analyses were conducted for different blade pitch angles, blade support conditions, number of blades, rotational speeds and freestream Mach numbers. A finite element model of the blade was used to determine the blade's vibration behavior and sensitivity to support stiffness. The calculated frequencies and mode shapes obtained with this model agreed well with the published experimental data. A computer code recently developed at LeRC and based on three-dimensional, unsteady, lifting surface aerodynamic theory was used for the aeroelastic analysis to examine the blade's stability at a cruise condition of Mach 0.8 at 1700 rpm. The results showed that the blade is stable for that operating point. However, a flutter condition was predicted if the cruise Mach number was increased to 0.9.

INTRODUCTION

One of the major research and technology programs at NASA Lewis Research Center is the Advanced Turboprop Program [1]. The goal of this effort is the development of turboprop (also known as propfan) propulsion systems which would have significant gains in fuel economy over turbofans without sacrificing aircraft performance. An important phase of this program is the Large-Scale Advance Propfan Program (LAP). This program involves the development, and both ground and flight testing of a complete eight bladed, 2.743 m (9 ft) diameter rotor system (Fig 1).

The SR7L advanced turboprop used in the LAP program is designed for a Mach number of 0.80 at an altitude of 10.66 km (35,000 ft). A number of unique design features are used to improve propeller performance. Reference 2 details the blade operating conditions and the many unconventional features of the SR7L design, such as thin, highly-swept and twisted, composite material blades of low aspect ratio and high disk solidity.

Research efforts on the SR7L propfan at LeRC have focused on these properties, particularly with respect to improved structural modeling and aeroelastic analysis of the bladed propfan assemblies. Although a complete literature review is beyond the scope of this paper, some areas where new analytical techniques have been recently implemented include modeling of blades constructed with composite materials [3], and geometric nonlinear analysis of flexible rotating blades [4,5,6]. A new three-dimensional, steady and unsteady aerodynamic theory for propfans with subsonic leading edge, has been developed in Reference 7.

This paper presents the structural and aeroelastic analysis of the SR7L advanced propfan incorporating the aforementioned techniques. The principle objectives of this study are to perform parametric studies of the SR7L propfan to determine the correct support stiffness values for use in the blade finite element model; to use the resulting model to calculate the vibration characteristics at the design rotational speed; and then to calculate unstalled flutter stability at the design condition, as well as to examine the cascade effects on the blade's stability. The finite element code MSC/NASTRAN was used to calculate the vibration characteristics of the blade. This information was then used in conjunction with the computer program ASTROP (Aeroelastic STability and Response of Propulsion Systems), a recently developed modal flutter code described in Reference 8, for the aeroelastic stability studies.

As a flight worthy test model, the SR7L propfan is being used in the Propfan Test Assessment (PTA) flight test program to investigate basic configurations, critical speed frequency margins, and aerodynamic performance (Fig 2). Consequently, it will provide an extensive experimental database for use in the assessment of analytical tools.

VIBRATION ANALYSIS

Since aeroelastic analyses are sensitive to blade frequencies and mode shapes, it is important that the blade finite element model and analysis accurately reflect it's modal characteristics. The vibration analysis of advanced turboprop blades is complicated by the fact that these swept and twisted blades will have relatively large and nonlinear steady deflections due to centrifugal forces. MSC/NASTRAN was chosen because it has the capability to perform geometric nonlinear analysis, as well as the capability to update the displacement dependent centrifugal forces. The frequencies and mode shapes required for the aeroelastic analysis are extracted from the final mass and stiffness matrices that correspond to the blade's centrifugally deformed position.

Model and Analysis Description

A previous study [9] of the SR7L propfan had used a finite element blade model based on a preliminary design. The NASTRAN finite element model used in this study is based on the final SR7L design [10]. The blade geometry and airfoil data were obtained from the engineering design drawings. The composite material properties were calculated by a micro-mechanics approach using available fiber and matrix properties obtained from actual testing of the material. Shell, adhesive, spar, and shell filler material were combined using the COmposite Blade STRuctural ANalysis (COBSTRAN) program to produce monolithic shell elements [3].

The finite element model used is shown in Figure 3. It has 261 nodes, 449 triangular shell elements (NASTRAN element CTRIA3), and five bar elements (NASTRAN element CBAR). Bar elements were used to model the shank. Multipoint constraint cards that couple the displacement of prescribed gird points, were used to define the shank/blade interface.

MSC/NASTRAN Solution 64 was used for the geometric nonlinear analysis [4]. This solver uses a modified Newton-Raphson algorithm to simulate the correct displacement versus load relationship. The algorithm iterations are controlled in Solution 64 through "subcases," with a minimum of two being required. The first subcase computes the initial, linear deflected shape. Subsequent subcases, or iterations, then use the previously deflected shape to compute the differential stiffness matrix along with the new set of displacements. Enough iterations should be specified to obtain a converged, displacement vector. For this analysis, 14 iterations, or subcases, were used.

Solution 64 was further augmented to perform a combined nonlinear displacement, frequency, and mode shape analysis by NASTRAN DMAP Alters to the Solution 64 Case Control and Bulk Data Decks. These DMAP Alters use the final mass and stiffness matrices computed in the geometric nonlinear analysis and access eigenvalue extraction routines that solve for the frequencies and modes shapes. The advantages of this technique were reduced CPU time (roughly one-half), quicker turnaround time, reduced output, and no need to create a Solution 63 normal modes analysis input deck, nor use the

Cray DBASE facility to store the mass and stiffness matrices Solution 63 requires. Reference 6 details the DMAP Alter cards necessary for this technique. It should be noted that the Coriolis forces were not included for the normal modes analysis since they have been found to be negligible for the case of thin, rotating blades [8].

Calculated Frequencies and Mode Shapes

To establish the validity of the finite element blade model for use with the aeroelastic studies, the calculated frequencies were compared with the experimental values. Frequencies and corresponding mode shapes were calculated at 1200 rpm over a range of blade setting angles from 35 to 60 degrees, and compared with those given in Reference 11. It should be noted that the calculated frequencies do not include the effect of steady airloads.

Figure 4 shows the first four calculated mode shapes with contour lines at a blade setting angle of 60 degrees. The contour lines shown are arbitrary displacements normal to the plane of rotation. Figure 5 gives an "animated" version of the mode shapes by superimposing the extreme deformed blade outlines with a few intermediate ones.

The first mode is seen to be predominantly a first bending mode with no nodal lines and fairly evenly spaced contours in the upper half of the blade. The second mode is predominantly a first edgewise mode, with most of the motion occurring near the tip in the chordwise direction. The third mode can be classified as the second bending mode, since there is a generally chordwise nodal line near the tip. The fourth mode can be classified as the first torsion mode since there is a midchord nodal line.

Figure 6 shows the comparison of the measured and calculated frequencies. There is very good agreement for the first mode, i.e., first bending, over the entire range of blade setting angles. The fourth mode frequencies, i.e., first torsion, similarly show acceptable agreement. However, there is a poor match with the second mode, first edgewise; as well as the third mode, second bending. For both cases, the calculated frequencies were higher than the measured frequencies.

Since the calculated second and third mode frequencies were much higher than the experimental ones, and the calculated fourth mode frequencies were also slightly higher, a parametric study was made to investigate the model of the blade constraints, and their effect on the blade's frequencies and mode shapes. The actual blade is retained in a hub by angular contact ball bearings set in races on the blade shank and integral races in the hub. To accurately simulate the blade/hub compliance, the blade constraints were modeled by using spring elements attached to the base of the blade shank. A total of four degrees of freedom for the shank base were allowed; translation along pitch change axis, bending rotations in and out of the plane of rotation, and rotation about the blade's pitch change axis. The blade shank was completely fixed for translations in directions other than the pitch change axis (Fig. 7).

Using the values suggested in Reference 12 for the original model of the blade support stiffnesses, parametric runs were made to examine the effect of varying these stiffnesses on natural frequencies and mode shapes. Figures 8a and 8b show the effect of the in-plane bending rotation (K_{R1}) and out-of-plane bending rotation (K_{R2}) support stiffnesses, respectively. The original stiffness value for each direction is also indicated. Each stiffness value was varied individually while the other values were held constant.

Variation of the K_{R1} stiffness (Fig. 8) about the value suggested in Reference 12 had little effect. The first two modes did have noticeable changes, but only over three orders of magnitude of stiffness changes. Although not shown, the pitching axis support stiffness (K_{R3}) and spanwise translational support stiffness had virtually no effect on the frequencies.

The effect of varying the stiffness value K_{R2} on frequencies is shown in Figure 8b. Large, significant changes occurred in the frequency values for the first edgewise mode. Frequencies for the first and second bending modes, and first torsional modes were relatively unaffected. Figure 8b illustrates that the edgewise mode could be selected to be the second, third, or fourth mode, depending on the out-of-plane bending stiffness value.

Figure 9 shows how the blade tip modal displacements and frequencies, as viewed down the blade span, change as the out-of-plane bending stiffness is increased. Figure 9a shows the second mode to be clearly the first edgewise mode as the motion is nearly all in the chordwise direction. The first and third modes can be characterized as the first and second bending modes from the amount of blade normal displacements. Figure 9b shows the second mode from the first crossover region from Figure 8a (K_{R2}=1.514 E06 m-N/rad) to still have a fair degree of chordwise motion, although the leading edge area does have a some blade normal motion. Note that the third mode now also contains a degree of chordwise motion. Figure 9c shows the tip mode shapes from the second crossover region in Figure 8b (K_{R2}=1.13 E08 m-N/rad). The second mode can be classified a second bending mode due to the predominate blade normal displacements. The third mode is clearly the first torsional mode, while the fourth mode appears to be the first edgewise mode due to the chordwise motion at the leading edge.

Figures 8b and 9b clearly show that the originally suggested values for K_{R2} cause the second and third modes to occur in a transition region between the first edgewise and second bending modes. This helps to account for the difference between the experimental and calculated second and third mode frequencies in Figure 7. The experimental edgewise mode is much lower than the calculated one; reflecting that mode's strong sensitivity to the support stiffness. The narrow range of values for the calculated second and third modes, and even the experimental third mode, also illustrate the effect of the support stiffness within the crossover region.

From the parametric studies, values for the support stiffnesses were selected so that a "tuned support" model was developed. This was done in an attempt to give the best overall agreement between the calculated and measured frequencies. It was decided to try to soften the support stiffnesses since the

edgewise, second bending, and torsional frequencies were too high. Table 1 gives the support stiffness values used in the original model and the tuned model. K_{R1} was chosen at 4.52 E05 m-N/rad because this seemed to be the minimum value above which there were very little changes in the blade's frequencies. K_{R2} was chosen slightly lower at 9.04 E05 m-n/rad because this was the value that gave the best agreement with the experimental edgewise mode without greatly affecting the other three modes. Since the K_{R3} value seemed to have very little effect on the frequencies, it was purposely chosen to be very low (1.13 E02 m-N/rad).

Figure 10 shows the effect of blade setting angles on calculated frequencies at 1200 rpm, using the tuned support over the same range of blade setting angles as before. The effect of the softer support springs are immediately evident. The first mode frequencies are slightly lower. However, the second, third, and fourth modes show much better agreement than before, especially near the operational blade setting angle of 58^{o}.

Figure 11 shows the effect of rotating speed on natural frequencies for the two models. Due to the softer support, the tuned model's frequencies are generally lower (<10%) than the original model's. For the three modes that will most affect flutter; first and second bending, first torsion; there is generally better agreement between calculated and measured results at the design speed (1700 rpm) using the original model. This is contrast to Figures 6 and 10, which showed a better overall agreement at 1200 rpm, using the tuned, softer support.

A possible explanation for the difference is that at the higher speed, the blade shank had seated itself better, resulting in a stiffer support. This is supported by the fact that the measured frequencies showed a greater degree of change between the two test speeds than either of the finite element models. This type of nonlinear support would be impossible to model accurately over a wide range of speeds using linear, spring elements.

Since Figure 11 does show acceptable agreement between calculated and measured frequencies, it was decided that the original model was suitable for the aeroelastic studies. However, it was decided to use the tuned support model for some parametric flutter studies also. This way, the influence of the softer modes, particularly first edgewise and second bending, on the blade stability could be investigated.

FLUTTER ANALYSIS

As mentioned previously, the structural analyses provided frequencies and mode shapes that were input for the aeroelastic analysis. The modal flutter code ASTROP3 was used to calculate the aerodynamic damping for each mode of vibration. The following sections briefly discuss the aero code that was used, and detail the parametric studies.

Flutter Analysis Method

The ASTROP3 code is a normal mode analysis method that was developed for the analysis of propulsion blading. It is based on three-dimensional, unsteady aerodynamics. A detailed explanation of the program is given in Reference 8.

The code described in References 7, 8, and 13, uses three-dimensional subsonic (Mach number of relative flow is less than unity), unsteady aerodynamics. However, for the SR7L configuration at a design freestream Mach number 0.80 and a rotational speed of 1700 rpm, the Mach number of relative flow at the tip is more than one. To calculate the unsteady aerodynamics for supersonic Mach numbers, the aerodynamic model described in [7] has been extended in [13].

The cascade aeroelastic stability is determined by solving the dynamic system's eigenvalue problem. System damping and damped frequency are represented by the real and imaginary parts of the complex eigenvalue, respectively. Flutter occurs when the real part of the eigenvalue is greater zero. The damping ratio, as used in vibration engineering, can be calculated by dividing the real part by the magnitude of the complex eigenvalue.

The SR7L blade was analyzed at 1700 RPM, 57.7 degree blade setting angle, at the design altitude, and with varying Mach numbers. Table 2 lists the various Mach numbers, effective tip velocities, and effective angles of attack considered in this study. An eight-bladed propfan configuration consisting of identical blades, was used for this study.

Stability Results

Figures 12 and 13 show the predicted aerodynamic damping (real part of the system eigenvalue) at the design speed as a function of freestream Mach number. To estimate the available flutter margin for the SR7L propfan, the aerodynamic damping for freestream Mach numbers greater than 0.8 were also calculated and included. The values shown are for the most unstable SR7L interblade phase angles for both the original and tuned support condition,

respectively. The blade was stable for both cases at the design point of Mach 0.8 and 1700 rpm at an altitude of 10.66 km (35,000 ft). There was also very little difference in the most unstable interblade phase angle identified.

Modes one and three are stable over the range of Mach numbers with only minimal differences between the two support cases. Mode two shows consistently low damping values since this is the first edgewise mode, and it always has small aerodynamic loads.

It is evident from these figures that the fourth mode became unstable at freestream Mach number of 0.89. The severity and type, i.e. fourth mode,of the instability at that point, however, is questionable. The validity of this aerodynamic theory is still being investigated for transonic regions at which the SR7L instability is predicted. Also, from the similarity of Figures 12 and 13, there seems to be little effect of the blade support stiffness values used on the calculated aerodynamic damping as long as there was generally good agreement between the bending and torsional frequencies.

The values shown in these two figures are considered to be conservative, since neither material nor friction damping due to the hub constraint has been included in the analysis. Additional system damping would only have a stabilizing effect. From these results, it is concluded that the SR7L propfan is free from flutter at the design point.

Figure 14 shows a comparison of the ASTROP3 damping results ratio for the original stiffness model with those given in Reference 8. That study had used a modal flutter aero code solver, ACA, available in COSMIC/NASTRAN. The ACA code utilizes the two-dimensional, subsonic cascade aerodynamic theory of Jones and Rao applied in a strip theory manner [14]. The important feature of this figure is that the calculated damping was qualitatively similar to that in Reference 8; with the first mode being much more stable than either the second or third modes, and the third mode showing the least damping. A direct comparison of the values for the critical damping cannot be made due to differences in the aerodynamic theories used, as well as two slightly different blade designs. The finite element blade model used in Reference 8 was based on a preliminary blade design, and had higher third and fourth mode (second bending and first torsion) frequencies, 111.6 and 160.7 Hz versus 97.9 and 137.0 Hz, respectively, than the final blade design.

Cascade Effects

To illustrate the effects of cascade aerodynamics on flutter, parametric studies were made varying the number of blades in the propfan assembly. Figure 15 shows that the effect of the number of blades on modal damping is significant; with the first and third mode aerodynamic damping decreasing by 25% and 16%, respectively. Figure 16 is an example of a root locus plot of just the first mode interblade phase angles. It demonstrates the de-stabilizing influence of the cascade effect, as the length of the semi-major axis of the ellipse increases with additional blades. Also note that the flutter frequency is being reduced with increased blading.

SUMMARY OF RESULTS

1. Bending and torsional frequencies were generally insensitive to the support stiffness used. However, the blade edgewise frequencies were particularly sensitive to the out-of-plane bending support stiffness used.

2. With the exception of the edgewise mode, there was generally good agreement between calculated and experimental frequencies at the design speed. From the available test information, it appeared as if the blade hub constraint stiffness acted in non-linear manner with respect to rotational speed. This made it difficult to model the blade constraint condition with linear spring elements over a wide range of speeds.

3. The blade was stable at its design point of Mach 0.8 and 1700 rpm at altitude of 10.66 km (35,000 ft). The analysis did not consider any structural damping, which would only have a beneficial effect on stability.

4. A flutter point was found at an off-design condition of Mach 0.9 and 1700 rpm. The fourth mode (torsion) was unstable.

5. The blade support stiffness values had little effect on the calculated aerodynamic damping. This would imply that modeling efforts should be concentrated most on matching the in- and out-of-plane bending stiffnesses and obtaining reasonably close values (within 10%) for the bending and torsional modes.

6. Cascade effects were found to be considerable at the design point for configurations from two to ten blades, although an increase in the number of blades from eight to ten did not cause an instability for the configuration studied. (Note: normal propfan assembly consists of eight blades).

REFERENCES

1. Whitlow, J.B. Jr. and Sievers, G.K., "Fuel Savings Potential of the NASA Advanced Turboprop Program," NASA TM-79124, 1984.

2. Sagerser, D.A. and Ludemann, S.G., "Large-Scale Advanced Propfan (LAP) Program Progress Report," AIAA Paper 85-1187, presented at the AIAA/SAE/ASME/ASEE 21th Joint Propulsion Conference, Monterey, California, July 8-10, 1985.

3. Aiello, R.A. and Chi, S., "Advanced Composite Turboprops:Modeling, Structural and Dynamic Analyses," ASME Paper 87-GT-78, 1987.

4. NASTRAN Theoretical Manual, NASA SP-221(06), 1977.

5. Lawrence, C. and Kielb, R.E., "Nonlinear Displacement Analysis of Advanced Propeller Structures Using NASTRAN," NASA TM 82727, August 1984.

6. Lawrence, C., et. al., "A NASTRAN Primer for the Analysis of Rotating Flexible Blades," NASA TM 89861, May, 1987.

7. Williams, M.H. and Hwang,C., "Three-Dimensional Unsteady Aerodynamics and Aeroelastic Response of Advanced Turboprops," AIAA 27th Structures, Structural Dynamics, and Materials Conference, Part 2, New York, 1986, pp.116-124.

8. Kaza, K.R.V., et. al., "Analytical Flutter Investigation of a Composite Propfan Model," AIAA Paper 87-0738, presented at the AIAA/ASME/ASEE/AHS 28th Structures, Structural Dynamics, and Materials Conference, CA, April, 1987.

9. Hirschbein, M., et. al., "Structural and Aeroelastic Analysis of the SR7L Propfan," NASA TM 86877, March, 1985.

10. Chou, S. "SR7L Turboprop Blade Finite Element Model," Sverdrup Topical Report, March, 1986.

11. Turnberg, J., SR7L test results presented at the Advanced Turboprop Workshop, NASA LeRC, November, 1986.

12. Sullivan, W.E., Turnberg, J.E., Violette, J.A., "Large-Scale Advanced Propfan (LAP) Blade Design," NASA CR 174790.

13. Williams M.H., private communication on unpublished work, 1987.

14. Elchuri, V., et. al., "NASTRAN Documentation for Flutter Analysis of Advanced Turbopropellors," NASA CR 167927.

TABLE 1

SUPPORT STIFFNESS VALUES

	In-Plane Bending Rotation, m-N/rad (in-lb_f/rad) K_{R1}	Out-of-Plane Bending Rotation, m-N/rad (in-lb_f/rad) K_{R2}	Pitching Torsion m-N/rad (in-lb_f/rad) K_{R3}
Original Model	1.153 E06 (1.02 E07)	1.514 E06 (1.34 E07)	2.260 E07 (2.00 E08)
Tuned Model	4.520 E05 (4.00 E06)	9.040 E05 (8.00 E06)	1.130 E02 (1.00 E03)

TABLE 2

EFFECTIVE BLADE TIP VELOCITIES

Freestream Mach Number	Effective Tip Velocity (Mach Number)
.6	1.02
.7	1.08
.8	1.15
.9	1.22

$Beta_{3/4}$ = 57.9° degrees
Rotational speed = 1700 rpm
Altitude = 10.66 km
Speed of sound = 296.57 m/sec

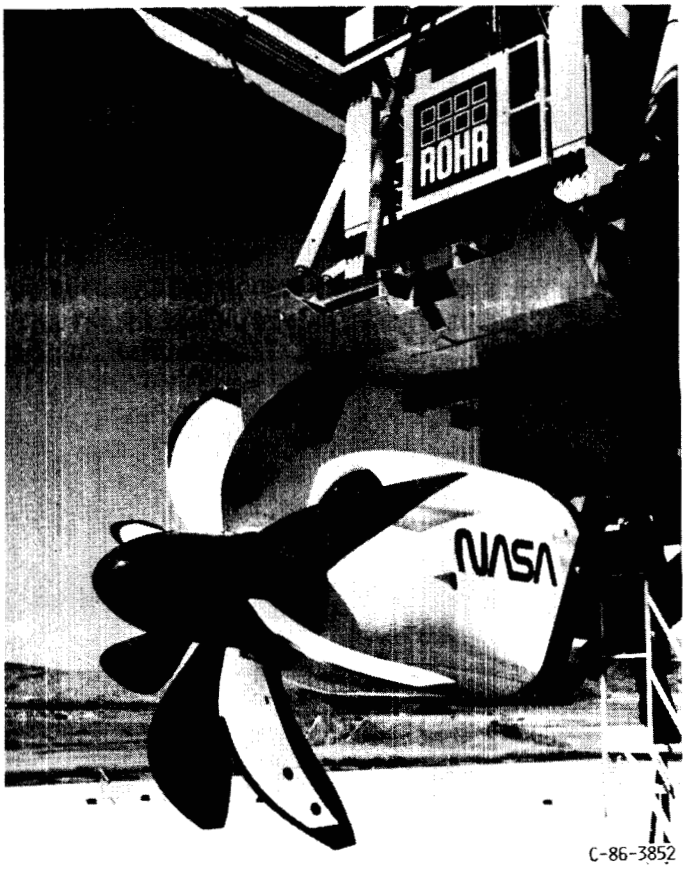

FIGURE 1. - SR7L PROP-FAN GROUND TEST CONFIGURATION.

FIGURE 2. - SR7L PROP-FAN FLIGHT TEST CONFIGURATION.

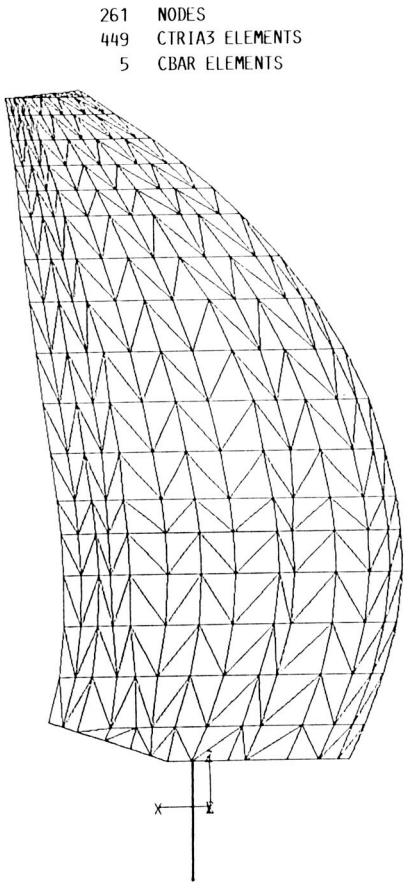

FIGURE 3. - FINITE ELEMENT MODEL OF THE SR7L PROP-FAN BLADE.

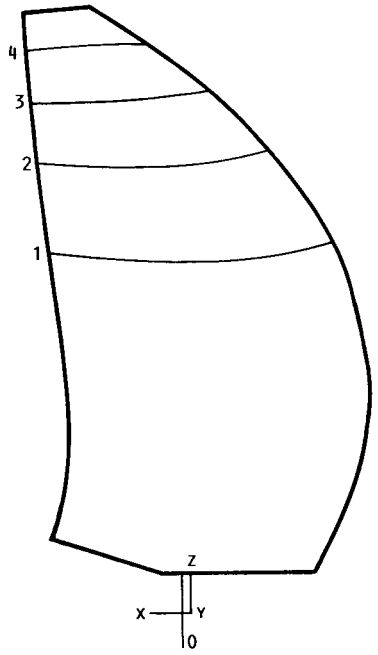

(A) FIRST MODE, 38.10 Hz, FIRST BENDING.

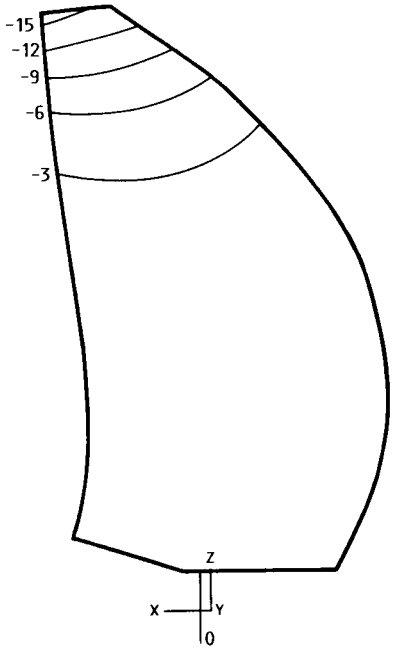

(B) SECOND MODE, 86.89 Hz, FIRST EDGEWISE.

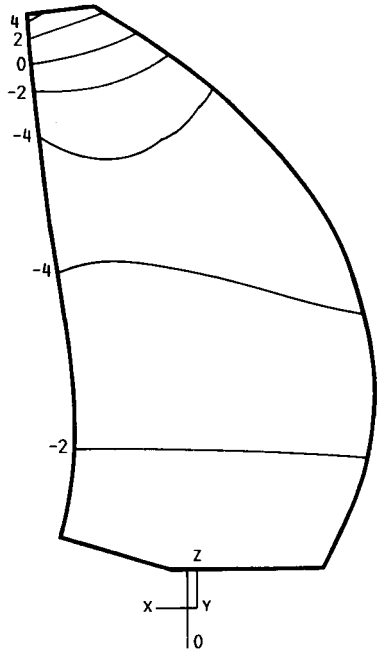

(C) THIRD MODE, 101.0 Hz, SECOND BENDING.

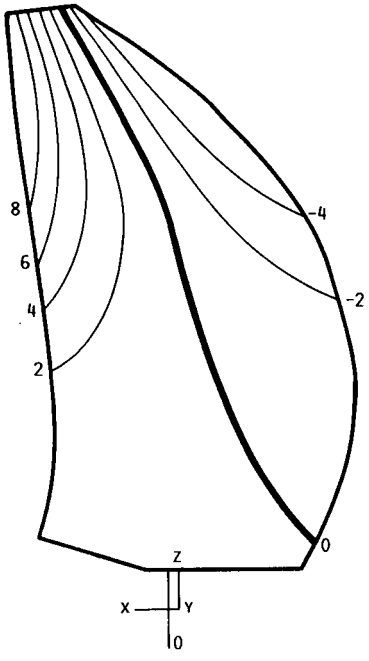

(D) FOURTH MODE, 160.9 Hz, FIRST TORSION.

FIGURE 4. - CALCULATED MODE SHAPES AT 1200 RPM (CONTOUR LINES SHOWN ARE NORMAL TO THE PLANE OF ROTATION).

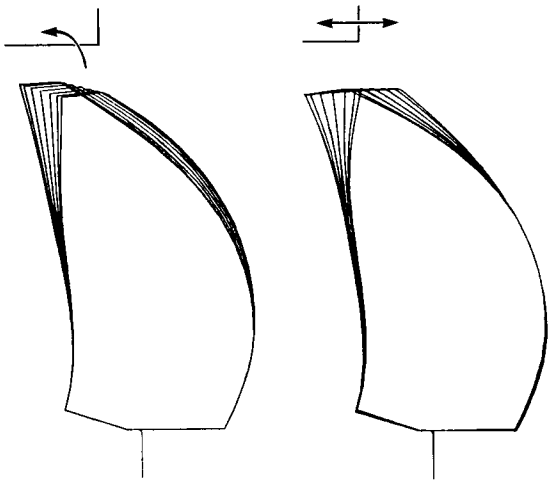

(A) FIRST MODE, FIRST BENDING.

(B) SECOND MODE, FIRST EDGEWISE.

(C) THIRD MODE, SECOND BENDING.

(D) FOURTH MODE, FIRST TORSION.

FIGURE 5. - "ANIMATED" CALCULATED MODE SHAPES.

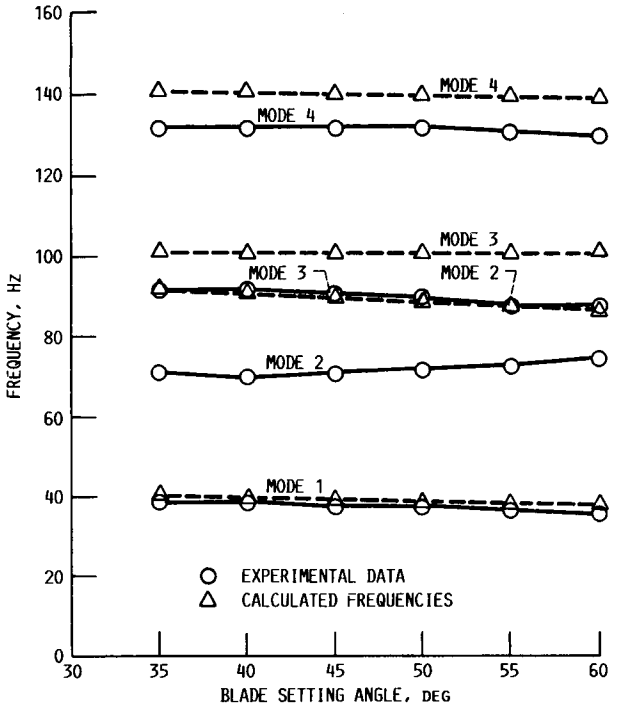

FIGURE 6. - SR7L FREQUENCY-VERSUS-SETTING ANGLE FOR 1200 RPM.

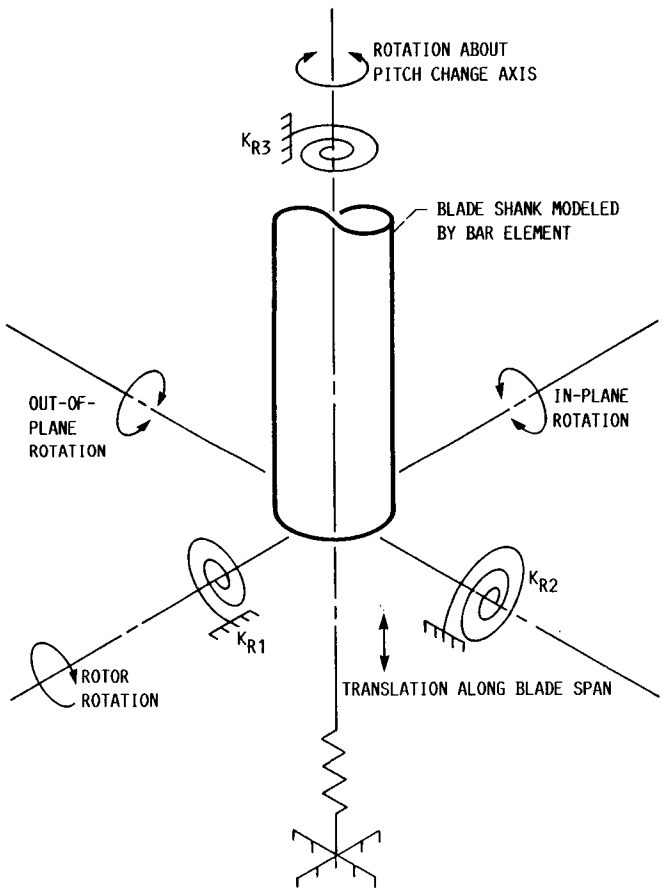

FIGURE 7. - BLADE SHANK CONSTRAINT MODEL.

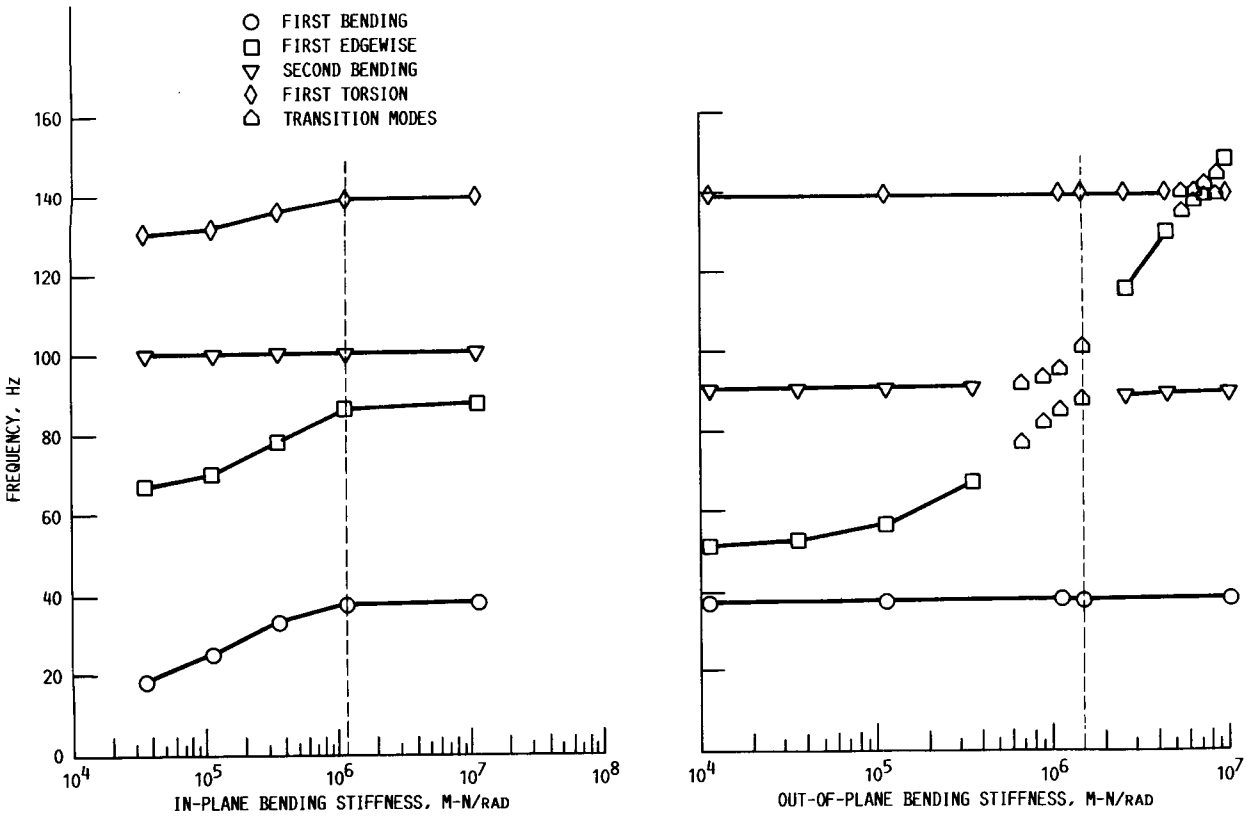

(A) IN-PLANE.

(B) OUT-OF-PLANE.

FIGURE 8. - SR7L FREQUENCIES VERSUS BENDING STIFFNESS.

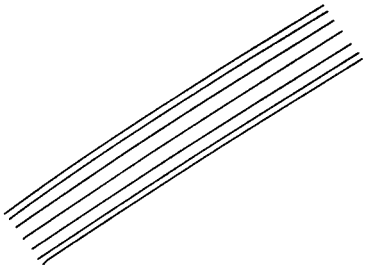

FIRST MODE, 37.47 Hz, FIRST BENDING

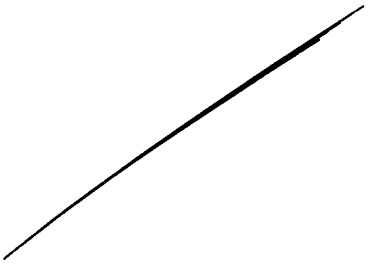

SECOND MODE, 50.99 Hz, FIRST EDGEWISE

(A) K_{R2} = 1.13 E3 M-N/RAD.

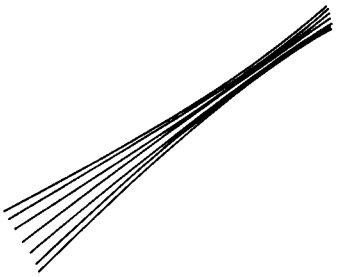

THIRD MODE, 90.94 Hz, SECOND BENDING

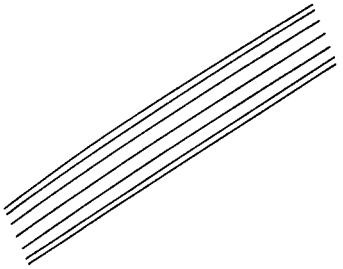

FIRST MODE, 38.52 Hz, FIRST BENDING

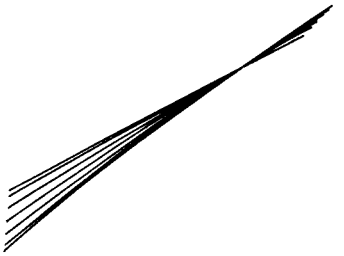

SECOND MODE, 87.62 Hz, FIRST EDGEWISE

(B) K_{R2} = 1.51 E6 M-N/RAD.

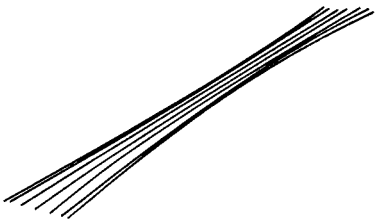

THIRD MODE, 101.9 Hz, SECOND BENDING

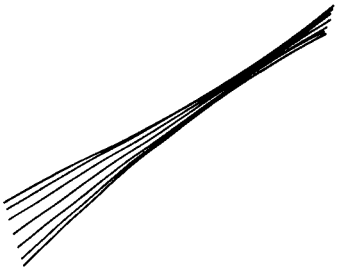

SECOND MODE, 89.97 Hz, SECOND BENDING

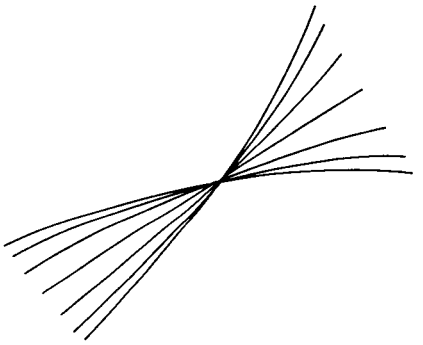

THIRD MODE, 139.2 Hz, FIRST TORSION

(C) K_{R2} = 1.13 E7 M-N/RAD.

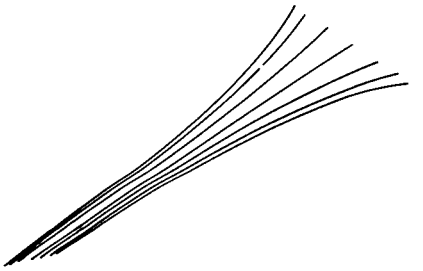

FOURTH MODE, 147.5 Hz, FIRST EDGEWISE

FIGURE 9. - BLADE MODAL DISPLACEMENT AT 3/4 RADIUS.

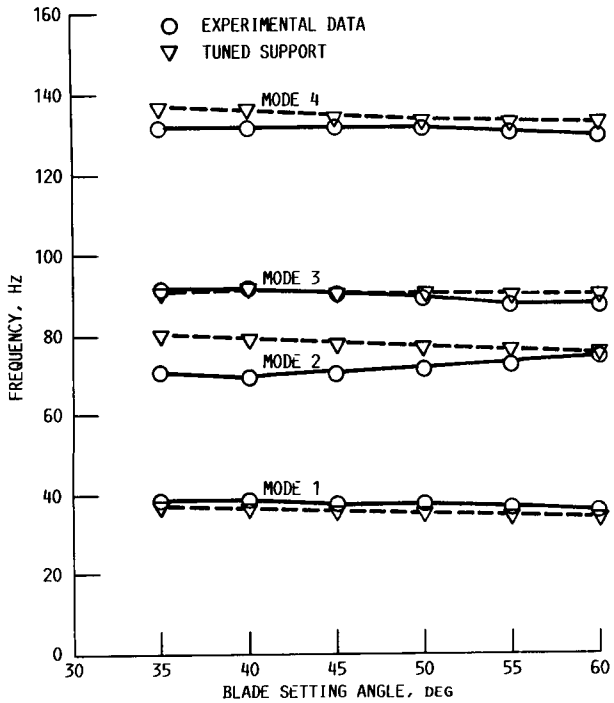

FIGURE 10. - SR7L FREQUENCY-VERSUS-SETTING ANGLE FOR TUNED SUPPORT.

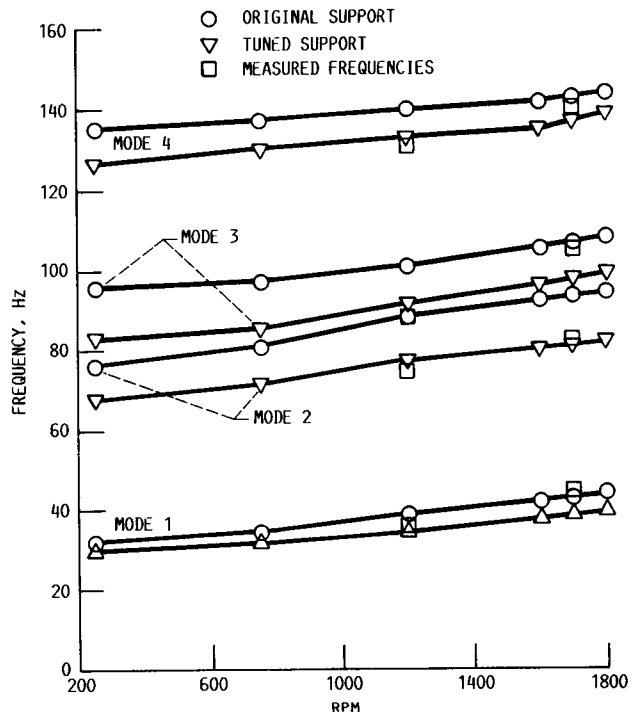

FIGURE 11. - SR7L FREQUENCY-VERSUS-RPM FOR ORIGINAL AND TUNED SUPPORT.

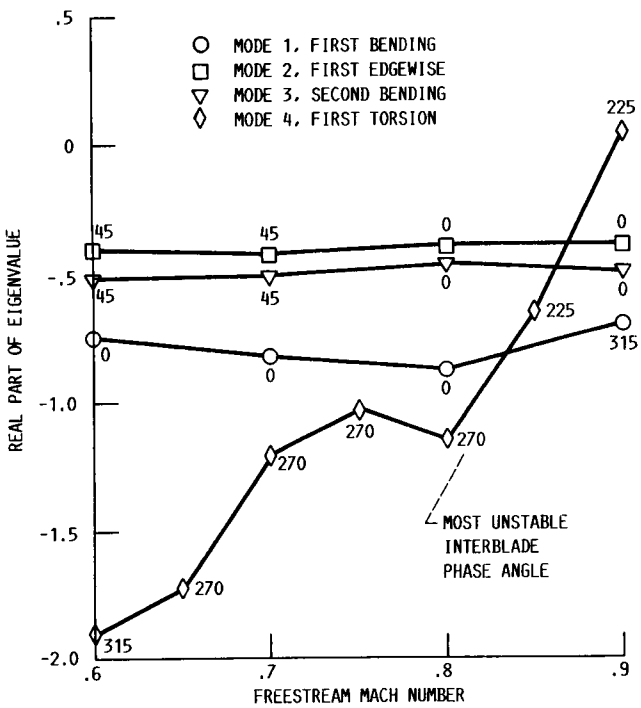

FIGURE 12. - SR7L DAMPING-VERSUS-MACH NUMBER FOR ORIGINAL SUPPORT.

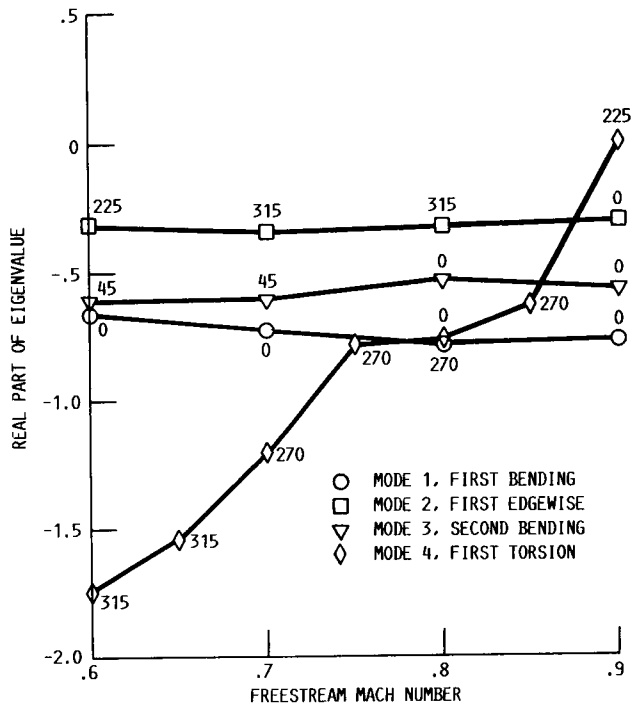

FIGURE 13. - SR7L DAMPING-VERSUS MACH NUMBER FOR TUNED SUPPORT.

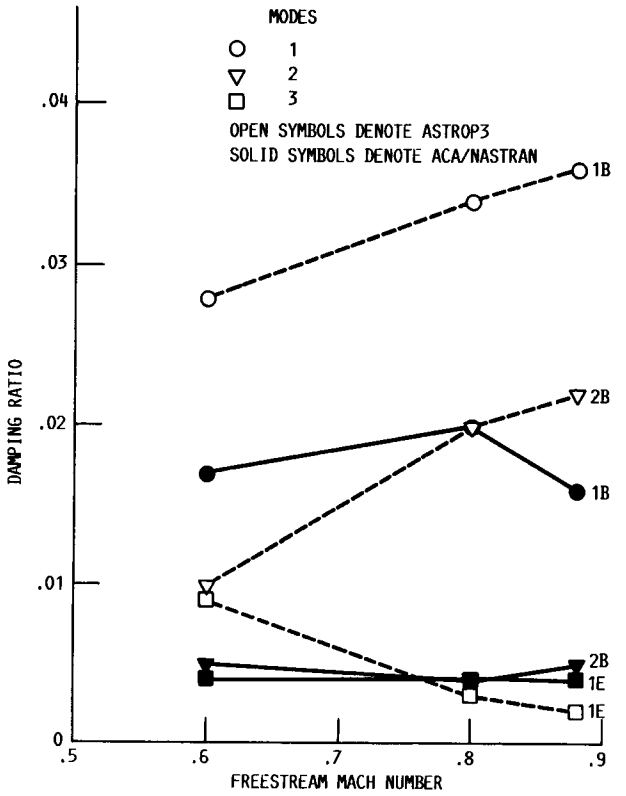

FIGURE 14. - SR7L CALCULATED MODAL DAMPING.

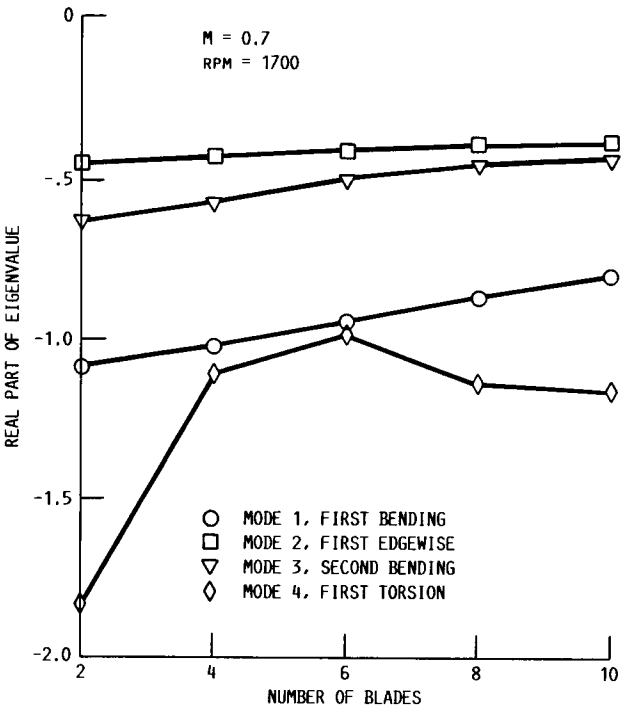

FIGURE 15. - CASCADE EFFECTS AT DESIGN POINT.

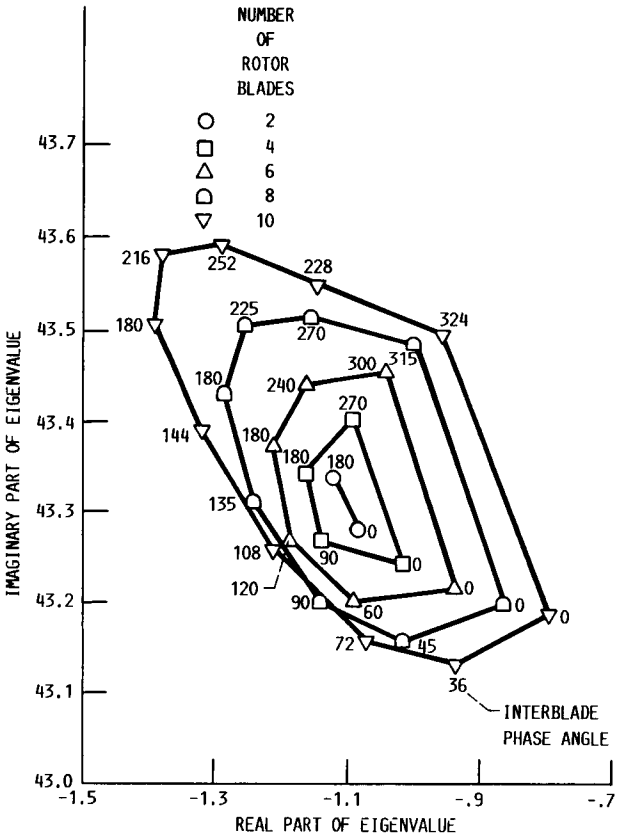

FIGURE 16. - MODE ONE ROOT LOCUS PLOT WITH CASCADE EFFECTS.

NASA
National Aeronautics and Space Administration

Report Documentation Page

1. Report No.	2. Government Accession No.	3. Recipient's Catalog No.
NASA TM-100272		

4. Title and Subtitle	5. Report Date
Vibration and Flutter Characteristics of the SR7L Large-Scale Propfan	January 1988
	6. Performing Organization Code

7. Author(s)	8. Performing Organization Report No.
Richard August and Krishna Rao V. Kaza	E-3908
	10. Work Unit No. 535-03-01

9. Performing Organization Name and Address	11. Contract or Grant No.
National Aeronautics and Space Administration Lewis Research Center Cleveland, Ohio 44135-3191	
	13. Type of Report and Period Covered
12. Sponsoring Agency Name and Address	Technical Memorandum
National Aeronautics and Space Administration Washington, D.C. 20546-0001	14. Sponsoring Agency Code

15. Supplementary Notes

Richard August, Sverdrup Technology, Inc., Lewis Research Center, Cleveland, Ohio 44135; Krishna Rao V. Kaza, NASA Lewis Research Center.

16. Abstract

An investigation of the vibration characteristics and aeroelastic stability of the SR7L Large-Scale Advanced Propfan has been performed using a finite element blade model and an improved aeroelasticity code. Analyses were conducted for different blade pitch angles, blade support conditions, number of blades, rotational speeds, and freestream Mach numbers. A finite element model of the blade was used to determine the blade's vibration behavior and sensitivity to support stiffness. The calculated frequencies and mode shapes obtained with this model agreed well with the published experimental data. A computer code recently developed at NASA Lewis Research Center and based on three-dimensional, unsteady, lifting surface aerodynamic theory was used for the aeroelastic analysis to examine the blade's stability at a cruise condition of Mach 0.8 at 1700 rpm. The results showed that the blade is stable for that operating point. However, a flutter condition was predicted if the cruise Mach number was increased to 0.9.

17. Key Words (Suggested by Author(s))	18. Distribution Statement
Large-scale propfan Dynamic analysis Aeroelastic computer code Blade flutter	Unclassified - Unlimited Subject Category 39

19. Security Classif. (of this report)	20. Security Classif. (of this page)	21. No of pages	22. Price*
Unclassified	Unclassified	20	A02

*For sale by the National Technical Information Service, Springfield, Virginia 22161